PHYSICAL REVIEW D **80,** 023001 (2009)

Lyman-α transfer in primordial hydrogen recombination

Christopher M. Hirata*
Caltech M/C 350-17, Pasadena, California 91125, USA

John Forbes†
Caltech MSC 272, Pasadena, California 91126, USA
(Received 3 April 2009; revised manuscript received 18 June 2009; published 6 July 2009)

Cosmological constraints from the cosmic microwave background (CMB) anisotropies rely on accurate theoretical calculations of the cosmic recombination history. Recent work has emphasized the importance of radiative transfer calculations due to the high optical depth in the H I Lyman lines. Transfer in the Lyα line is dominated by true emission and absorption, Hubble expansion, and resonant scattering. Resonant scattering causes photons to diffuse in frequency due to random kicks from the thermal velocities of hydrogen atoms, and also to drift toward lower frequencies due to energy loss via atomic recoil. Past analyses of Lyα transfer during the recombination era have either considered a subset of these processes, ignored time dependence, or incorrectly assumed identical emission and absorption profiles. We present here a fully time-dependent radiative transfer calculation of the Lyα line including all of these processes, and compare it to previous results that ignored the resonant scattering. We find a faster recombination due to recoil enhancement of the Lyα escape rate, leading to a reduction in the free electron density of 0.45% at $z = 900$. This results in an increase in the small-scale CMB power spectrum that is negligible for the current data but will be a 0.9σ correction for *Planck*. We discuss the reasons why we find a smaller correction than some other recent computations.

DOI: 10.1103/PhysRevD.80.023001 PACS numbers: 98.70.Vc, 32.80.Rm, 98.62.Ra

I. INTRODUCTION

The cosmic microwave background (CMB) anisotropy has proven to be one of the most useful and robust cosmological probes. The most recent example has been the Wilkinson Microwave Anisotropy Probe (WMAP) satellite, which has provided key information on the composition of the high-redshift Universe, the distance to the surface of last scattering (via the acoustic peak position), cosmic reionization, and the primordial power spectrum [1–3]. The development of precision cosmology with the CMB will continue with the upcoming launch of the *Planck* satellite. *Planck* data will be essential for dark energy studies: its measurement of $\Omega_m h^2$ and $D_A(z = 1100)$ will be needed to break degeneracies with $w(z)$ in supernova data and set the length of the baryon acoustic oscillation standard ruler, and the primordial power spectrum will be needed to interpret tests of the growth of structure using weak lensing and clusters [4–6]. The measurement of the primordial spectral index n_s will be essential for constraining models of inflation; indeed it is the precision measurement of n_s from WMAP (and upper limits on tensors) that have opened the era of tests of inflaton potentials [3,7].

In addition to its versatility, one of the advantages of the CMB as a cosmological probe is that the generation of CMB anisotropies is understood from first principles: they arise due to linear perturbations on a homogeneous, isotropic background of baryons, photons, dark matter, and neutrinos. There are now several public codes that solve these equations and compute the angular power spectrum C_ℓ [8,9] and whose numerical accuracy has now been checked to 1 part in 10^3 [10]. However the photons and baryons interact via Thomson scattering, so these codes require as input the ionization fraction $x_e(z)$. This is a complicated nonequilibrium physics problem as one must track the level populations of recombining hydrogen and helium atoms, as well as following the effects of the emitted radiation and its reabsorption.

The first attempts to solve primordial recombination were carried out by Peebles [11] and Zel'dovich *et al.* [12], and the progress of CMB experiments has driven theorists to construct ever more accurate models of recombination. Most CMB codes in common use today obtain $x_e(z)$ from the RECFAST code by Seager *et al.* [13,14], which is based on the multilevel atom (MLA) approximation. The MLA follows the level populations of each type of atom considered (H I, He I, He II) under the influence of bound-bound and bound-free transitions. The optically thick lines (the H I Lyman series and its He I and He II analogues) are treated using the Sobolev approximation [15] to avoid the need to track the radiation field explicitly. Two-photon decays from the H I $2s$, He I 2^1S_0, and He II $2s$ levels and their inverse process (two-photon absorption) are important and also included.

The picture that emerged from this work is one in which hydrogen recombination occurs far more slowly than the

*chirata@tapir.caltech.edu
†forbes@caltech.edu

Saha equation predicts. The reason is the production of radiation: a hydrogen atom that recombines directly to the ground level ($1s$) emits a Lyman continuum photon. Once ~ 1 out of every 10^8 H atoms has recombined the Universe becomes optically thick to this radiation and each direct recombination is immediately followed by an ionization. Recombination can therefore occur only indirectly, via recombination to the H I excited levels (nl, $n \geq 2$) and radiative cascade to $1s$. But here another bottleneck occurs: the buildup of radiation in the Lyα ($2p \rightarrow 1s$, 1216 Å) line. In the absence of a sink for Lyα photons, a hydrogen atom in the $2p$ level can only reach the ground level by exciting another hydrogen atom to $2p$. The intense thermal CMB radiation during the recombination epoch is easily capable of ionizing a hydrogen atom from the $n = 2$ level, so again the process produces no net recombinations. The two major processes that break the bottleneck are (i) the cosmological redshifting of photons out of the Lyα line, and (ii) the $2s \rightarrow 1s$ two-photon decay (the photons have a continuous energy distribution and hence are not immediately reabsorbed in hydrogen lines). Similar physics applies at earlier epochs to helium recombination, albeit with some additional complications due to the more complex energy level structure.

In the past several years, many authors have reinvestigated the recombination problem with attention to small physical effects, in particular, neglected pathways that might allow hydrogen atoms to reach the $1s$ level. In particular, the *Planck* mission will require much better accuracy than was desired in 1999 when the original version of RECFAST was written. The new effects considered have included two-photon decays from the ns and nd levels of H I [16–20] and the n^1S and n^1D levels of He I [16,17,21]; H I continuum absorption of He I 584 Å line radiation [22–24]; stimulated two-photon decays and two-photon absorption [19,25,26]; Raman scattering [19,21]; resolution of the H I l-sublevels [27]; and forbidden transitions in He I [17,22,23,28]. In some cases the corrections to the C_ℓs were $>1\%$, sufficient to bias the n_s measurement from *Planck* by several sigma [29]. Some of these corrections are now incorporated into the most recent version of RECFAST [30].

An additional correction is the deviation from strict Sobolev behavior in the very optically thick H I Lyα line ($2p \rightarrow 1s$). This is the subject of this paper. The Sobolev approximation is based on the assumptions of (i) identical absorption and emission profiles, (ii) complete frequency redistribution in each line scattering, (iii) absence of any other absorption or emission processes active in the same frequency range as the line, and (iv) quasistationarity, i.e. that the level populations and radiation field change little during the time it takes for a photon to redshift through the line. None of these approximations are quite valid during the recombination era. Previous authors have relaxed some of these assumptions individually, but there exists no comprehensive treatment. Krolik [31,32] considered the partial redistribution during Lyman-α scattering, and found only a small correction due to atomic recoil. Rybicki and dell'Antonio [33] relaxed the quasistationary assumption and found that the relaxation time scale for the Lyα line was a factor of a few shorter than the recombination time; in the context of modern experiments this would probably imply a significant correction to the recombination history. Hirata and Switzer [21] argued in the context of the He I 584 Å line that the deviation of absorption versus emission profiles would lead to a somewhat increased escape probability, an effect which was verified to be important for H I Lyα by Hirata [19]. There are also recent treatments of diffusion and atomic recoil by Grachev and Dubrovich [34] and quasistationarity by Chluba and Sunyaev [35]. However there is not yet a treatment relaxing all of (i–iv) simultaneously.

In this paper, we will first review the physics of the recombination era with an emphasis on the role of Lyα escape (Sec. II). Next we describe a numerical method for solving the Fokker-Planck equation in the vicinity of Lyα and grafting it on to an existing MLA code, and present the results obtained by this technique (Sec. III). We then describe an analytic approach to the Lyα escape, which is much simpler than the fully numerical technique and captures the essential physics (Sec. IV). We describe implications for precision CMB observations in Sec. V. We conclude in Sec. VI. Appendix A describes computation of two special functions $\chi(W, S)$ and $\mathcal{I}(W, S)$ introduced in this paper.

For ease of comparison, we use the same fiducial cosmology as in Ref. [19]: $\Omega_m h^2 = 0.13$, $\Omega_b h^2 = 0.022$, $T_{\rm CMB} = 2.728$ K, helium mass fraction $Y = 0.24$, and an effective number of massless neutrinos $N_\nu = 3.04$. We draw heavily on the work of Hirata [19], where our MLA code was first presented.

II. BACKGROUND

In this section, we begin with a review of the basic definitions (Sec. II A). We then review the MLA method and its extension to two-photon transitions (Sec. II B). We then describe the physical formulation of the Lyα diffusion problem (Sec. II C).

A. Definitions

Since this paper extends the code of Hirata [19], we begin with the same notation and basic equations as in that paper, and add new variables as needed for the Lyα problem. The total density of hydrogen nuclei is $n_{\rm H} \propto a^{-3}$ where a is the scale factor. Ionization fractions are given by the free electron abundance $x_e \equiv n_e/n_{\rm H}$ and free proton abundance $x_p \equiv n_p/n_{\rm H}$ relative to hydrogen. Since this paper concerns the epoch after completion of helium recombination and before any hydrogen converts to molecular or intermediate (H^-, H^{2+}, etc.) forms, we have $x_e = x_p$.

Photons are described by the phase space density $f(E)$. The abundance of specific energy levels of the hydrogen atom will be given by $x_{nl} = n[\mathrm{HI}(nl)]/n_{\mathrm{H}}$. Level degeneracies $g_{nl} = 2(2l+1)$, energies $E_{nl} = -h\mathcal{R}/n^2$, and Einstein coefficients A_{ij} have their usual meaning; we denote the hydrogenic Rydberg (in frequency units) by $\mathcal{R}$, and set Boltzmann's constant equal to 1 so that temperature has units of energy.

B. Multilevel atom and two-photon transitions

The Hirata [19] code follows bound-bound and bound-free transitions involving each level of H I. The treatment of bound-free transitions and of the matter temperature is not altered by this paper and the corresponding equations will not be repeated. For the bound-bound case, the rate equation is

$$\dot{x}_i|_{\mathrm{bb}} = \sum_{j>i} A_{ji} P_{ji} \left[(1 + f_{ji+}) x_j - \frac{g_j}{g_i} f_{ji+} x_i \right] + \sum_{j<i} A_{ij} P_{ij} \left[\frac{g_i}{g_j} f_{ij+} x_j - (1 + f_{ij+}) x_i \right], \quad (1)$$

where the sums are over levels j that are above ($j > i$) or below ($j < i$) the energy of level i, and f_{ji+} is the phase space density on the blue side of the line connecting levels i and j. The escape probability P_{ji} is expressed in terms of the Sobolev optical depth τ_{ji} via

$$P_{ji} = \frac{1 - e^{-\tau_{ji}}}{\tau_{ji}}, \quad (2)$$

and the optical depth is

$$\tau_{ji} = \frac{c^3 n_{\mathrm{H}}}{8\pi H \nu_{ji}^3} A_{ji} \left(\frac{g_j}{g_i} x_i - x_j \right). \quad (3)$$

Of particular importance to us is the optical depth in the Lyα ($2p \rightarrow 1s$) line, which is typically of order 10^8–10^9.

The phase space density f_{ji+} on the blue side of each line is required since these photons redshift into the line and can be absorbed or cause stimulated emission. In most cases it can be treated as a blackbody, but in the case of the Lyman series lines one must consider the nonthermal nature of the radiation field. In particular, photons emitted in the Lyβ line (1026 Å) will eventually redshift into Lyα and begin exciting atoms. This "feedback" process [22,36] is taken into account by looking up the phase space density that emerged from Lyβ at a previous epoch and taking this as input for the Lyα calculation.

Two-photon decays of the form

$$\mathrm{H}(nl) \rightarrow \mathrm{H}(1s) + \gamma + \gamma \quad (4)$$

produce photons at a rate per unit frequency per H atom of

$$\Delta_{nl}(\nu) = \frac{d\Lambda_{nl}}{d\nu} \left[(1 + f_\nu)(1 + f_{\nu'}) x_{nl} - \frac{g_{nl}}{g_{1s}} f_\nu f_{\nu'} x_{1s} \right], \quad (5)$$

where $d\Lambda_{nl}/d\nu$ is the spontaneous two-photon decay rate. One can easily incorporate the total decay rate

$$\dot{x}_{nl}|_{2\gamma} = -\int_{(1-n^{-2})\mathcal{R}/2}^{(1-n^{-2})\mathcal{R}} \Delta_{nl}(\nu) d\nu \quad (6)$$

in the system of ordinary differential equations (ODEs) for the excited levels. However one must also take account of the radiation produced: if one of the emitted photons has an energy exceeding Lyα, it will eventually redshift into the Lyα resonance and excite a hydrogen atom. This is done by the virtual level method [19], which implements Eq. (4) by introducing *purely as a mathematical device* a new virtual level of the hydrogen atom with energy $E_{1s} + h\nu$ (where ν is the frequency of the higher-energy photon) and infinitesimal degeneracy. The decay in Eq. (4) can then be treated as a sequence of one-photon decays. The required choice of effective one-photon rate coefficients required for this procedure to work are given in Sec. IVA of Ref. [19]; these choices also account for two-photon absorption. The same procedure also applies to other two-photon processes such as Raman scattering and two-photon recombination/ionization. Most importantly, the same feedback machinery used for one-photon transitions is automatically applied to the two-photon transitions.

The two-photon differential decay rate $d\Lambda_{nl}/d\nu$ contains resonances associated with the allowed one-photon decays. For example, the two-photon decay rate from $3d \rightarrow 1s$ has a resonance corresponding to the sequence

$$\begin{aligned} \mathrm{H}(3d) &\rightarrow \mathrm{H}(2p) + \gamma(\mathrm{H}\alpha), \\ \mathrm{H}(2p) &\rightarrow \mathrm{H}(1s) + \gamma(\mathrm{Ly}\alpha). \end{aligned} \quad (7)$$

These resonances are physical since such decays actually do produce two photons [18]. They do however result in very large decay rates if one naively computes the quantity

$$\Lambda_{3d}^{\mathrm{tot}} = \frac{1}{2} \int_0^{8\mathcal{R}/9} \frac{d\Lambda_{3d}}{d\nu} d\nu = 6.5 \times 10^7 \ \mathrm{s}^{-1} \quad (8)$$

(compare to 8.2 s^{-1} for the $2s$ level). Naively the existence of such a rapid $3d \rightarrow 1s$ two-photon decay process would dramatically accelerate recombination, but since most of these decays produce photons within the Lyα line this turns out not to be the case: almost every $3d \rightarrow 1s$ two-photon decay is immediately undone by Lyα absorption. Ultimately the inclusion of these two-photon decays produces only $\mathcal{O}(1\%)$ corrections to the recombination history when one tracks the radiation field as well [19]. It is important to note that this result can only be obtained by consideration of radiative transfer in the Lyα line [17,18].

Overall, this yields a system of ODEs for the atomic level populations. These have explicit dependence on their history so the results of the integration must be stored for

future reference. Time steps are equally spaced in $\ln a$, with a fiducial choice of $\Delta \ln a = 4.25 \times 10^{-5}$. The excited atomic levels are treated using the steady-state approximation, i.e. assuming that the atom reaches the ground state or is ionized in a time short compared to the recombination time scale.

C. The Lyα diffusion problem

The treatment of radiative transfer in the Lyman series described in Sec. II B correctly describes many processes. It contains correct emission and absorption profiles for all of the Lyman lines, including interference between neighboring resonances, and is fully time-dependent. However, one key piece of physics is missing: it neglects the Doppler shift due to the motion of the atoms. For continuum processes far from resonance this is a minor error. It is a major omission in the vicinity of the Lyman lines, where repeated scattering of photons off of hydrogen atoms can cause them to undergo a random walk in frequency (frequency diffusion). This is especially true for Lyα because of its very high scattering-to-absorption ratio. This section is devoted to a qualitative discussion of the physical processes involved; quantitative computations are deferred to Sec. III.

The behavior of the radiation intensity near the Lyα line is a competition among several effects. The resonant scattering of photons off of hydrogen atoms,

$$\mathrm{H}(1s) + \gamma \rightarrow \mathrm{H}(2p)_{\mathrm{virtual}} \rightarrow \mathrm{H}(1s) + \gamma, \tag{9}$$

allows photons to exchange energy with the kinetic degrees of freedom of the matter but does not change the number of photons in the Lyα resonance. Therefore if only this process were active it would drive the radiation intensity toward a modified blackbody $f_\nu = [e^{(h\nu-\mu)/T_{\mathrm{m}}} - 1]^{-1}$ where the chemical potential μ is a constant. Since near Lyα $f \ll 1$ the Bose-Einstein statistics of the photon are negligible and we expect $f_\nu \propto e^{-h\nu/T_{\mathrm{m}}}$. A second process is the Hubble expansion, which moves photons to lower frequency at a constant rate $\dot{\nu} = -H\nu$. A third process is the "true" emission and absorption of the Lyα photons—that is, emissions and absorptions that are not part of the scattering process [Eq. (9)]. In this case, the line profile approaches the form shown in Fig. 1: near line center the emission, absorption, and scattering are dominant. The emission and absorption set the phase space density of photons at line center to be that of equilibrium, $f(\nu_{\mathrm{Ly}\alpha}) = x_{2p}/(3x_{1s})$, and the scattering then gives the frequency dependence

$$f_\nu = \frac{x_{2p}}{3x_{1s}} e^{-h(\nu-\nu_{\mathrm{Ly}\alpha})/T_{\mathrm{m}}}. \tag{10}$$

At some frequency ν_{trans} sufficiently far to the red side of the Lyα line, a transition occurs where the time to redshift out of the line becomes shorter than the time to diffuse back to line center. Beyond this point, the phase space density approaches a constant $f_{\mathrm{Ly}\alpha-}$, which is related to the net flux of photons to the red side of the Lyα line via

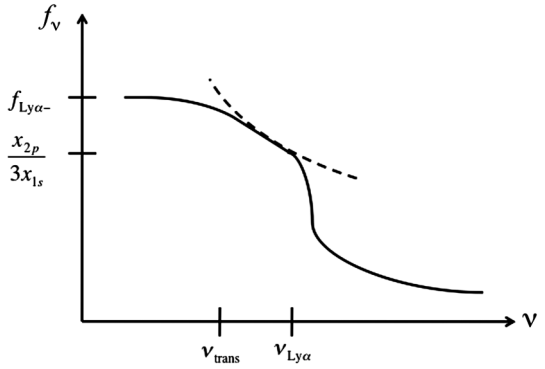

FIG. 1. A schematic representation of the photon phase space density near Lyα. The dashed line shows the chemical equilibrium solution, Eq. (10). The true solution (solid line) comes to equilibrium near line center. As one moves to the red side of the line, the rate of absorption, emission, and scattering decrease, and at some point ($\nu \sim \nu_{\mathrm{trans}}$) the photons fall out of chemical equilibrium and redshift out of the line.

$$\frac{d(\#\mathrm{photons})}{dVdt} = \frac{8\pi H}{\lambda_{\mathrm{Ly}\alpha}^3} f_{\mathrm{Ly}\alpha-}. \tag{11}$$

(Here $8\pi H/\lambda_{\mathrm{Ly}\alpha}^3$ is simply the number of photon modes per unit volume per unit time that redshift through the frequency $\nu_{\mathrm{Ly}\alpha} - \epsilon$.) Qualitatively, the rate at which photons redshift out of Lyα is determined by Eq. (10) at the transition frequency, combined with Eq. (11). This in turn gives the net $2p \rightarrow 1s$ decay rate (after a correction involving $f_{\mathrm{Ly}\alpha+}$ for photons that redshift *in* to Lyα and excite atoms is applied). In equations, we have

$$\dot{x}_{2p\rightarrow 1s} = \frac{8\pi H}{n_{\mathrm{H}} \lambda_{\mathrm{Ly}\alpha}^3} \left[\frac{x_{2p}}{3x_{1s}} e^{-h(\nu_{\mathrm{trans}}-\nu_{\mathrm{Ly}\alpha})/T_{\mathrm{m}}} - f_{\mathrm{Ly}\alpha+} \right]. \tag{12}$$

This equation with $\nu_{\mathrm{trans}} \approx \nu_{\mathrm{Ly}\alpha}$ and $f_{\mathrm{Ly}\alpha+} = (e^{h\nu_{\mathrm{Ly}\alpha}/T_{\mathrm{r}}} - 1)^{-1}$ gives the Peebles [11] transition rate, equivalent to the Sobolev rate in the limit of $\tau \gg 1$; an excellent description of the physics can be found in Sec. VI of the book by Peebles [37]. The same equation, with various estimates of the "effective" ν_{trans}, is the underlying conceptual reason for the accelerated recombination found by authors who considered repeated Lyα scattering [34]. (Recombination is accelerated rather than decelerated because $\nu_{\mathrm{trans}} < \nu_{\mathrm{Ly}\alpha}$.)

The role of emission and absorption in the Lyα damping wings must also be considered. It was at first argued that because the emission and absorption profiles are the same (they are both Voigt profiles), this process tends to smooth out the frequency dependence of f_ν and suppress the boost factor $e^{-h(\nu_{\mathrm{trans}}-\nu_{\mathrm{Ly}\alpha})/T_{\mathrm{m}}}$ in Eq. (12) [32]. However, true absorption of Lyα photons is actually a multiple-photon

process: the virtual H($2p$) atom must not decay back to the ground state, but rather absorb another photon, e.g.

$$\mathrm{H}(1s) + \gamma(\mathrm{Ly}\alpha) + \gamma(\mathrm{H}\alpha) \rightarrow \mathrm{H}(3s, 3d). \quad (13)$$

It follows that the Lyα absorption profile actually depends on the color temperature of the ambient CMB near Hα, because of energy conservation: if the first photon is from the red tail of Lyα then the second must be from the blue tail of Hα and vice versa. In contrast, the emission profile, i.e. the reverse of Eq. (13), is simply the Voigt profile (with small corrections due to neighboring resonances and stimulated emission). Thus in the cosmological context, the absorption profile is enhanced relative to the emission profile in the blue wing, and suppressed in the red wing, so true absorption and emission also tend to establish a red tilt to the radiation spectrum. We can also understand this effect thermodynamically: since true absorption of a Lyα photon followed by true emission (a process termed "incoherent scattering" by Krolik) exchanges the Lyα photon's energy with the low-energy Hα photons, it follows that this process also tends to drive the radiation spectrum toward a modified blackbody, but this time with temperature T_r. At high redshifts we have $T_\mathrm{r} \approx T_\mathrm{m}$ and so once again Eq. (10) should apply if true emission and absorption are dominant processes. Their consideration leads to a spectrum similar to that of Fig. 1 and hence to a transition frequency and enhanced redshifting rate just as does Lyα scattering. This effect has been seen in the consideration of two-photon decays; see e.g. Sec. VB of Ref. [19].

'A fourth process is the $2s \rightarrow 1s$ two-photon continuum: a small fraction of this continuum overlaps the red damping tail of Lyα (especially when modifications due to stimulated emission are considered) and this should be taken into account.

A complete theory of recombination must take full account of all these effects, and yield predictions for the $2p \rightarrow 1s$ decay rate and Lyα radiation profile. It should go well beyond the conceptual discussion of "ν_trans" and account for non-time-steady effects.

The basic strategy in both our numerical and analytical methods is to excise the region immediately surrounding the Lyα line from the aforementioned two-photon radiative transfer code and replace it with a method that solves the diffusion equation at high resolution. A hybrid method is necessary because the resolution required near Lyα (we must resolve the Doppler width of the line) would be too expensive if applied to the entire spectrum.

III. NUMERICAL METHOD

In our numerical method, we treat the photons near the Lyα using a time-dependent Fokker-Planck method. This replaces the complicated redistribution of photons with a partial differential equation (PDE) that can be solved numerically. We first set up this equation and its method of solution, and then comment on the initial and boundary conditions and interface to the MLA code. The Fokker-Planck and MLA codes are interdependent, since the Fokker-Planck code requires boundary conditions and level populations from the MLA code, whereas the MLA code needs the Fokker-Planck code to determine the Lyα decay rate and the flux of photons emerging from the red wing of Lyα. We solve this problem by alternately running each code until convergence is achieved. An interface script passes key variables between the two codes, such as the phase space density of photons that redshift across the frequency boundaries.

We divide the region of frequency near the Lyα into bins spaced equally in $\ln\nu$, usually with spacing $\Delta \ln\nu = 8.5 \times 10^{-6}$. This is fine enough that it takes many steps for a photon to redshift through a Doppler width (the condition is that $\Delta \ln\nu \ll \sqrt{T_\mathrm{m}/m_\mathrm{H}c^2}$). We denote by N_i the number of photons per H nucleus per frequency bin in the ith bin, and the frequency associated with the ith bin by ν_i. This is related to the phase space density via

$$N_i = \frac{8\pi\nu_i^3 \Delta \ln\nu}{c^3 n_\mathrm{H}} f(\nu_i). \quad (14)$$

This evolves with time according to Hubble redshifting, emission, absorption, and scattering:

$$\dot{N}_i = \dot{N}_i|_\mathrm{H} + \dot{N}_i|_\mathrm{em} + \dot{N}_i|_\mathrm{ab} + \dot{N}_i|_\mathrm{sc}. \quad (15)$$

We use $M = 2001$ bins in our standard case, and place the i_0^th bin [where $i_0 = \frac{1}{2}(M-1) = 1000$] at Ly$\alpha$ line center. Then

$$\nu_i = \nu_{\mathrm{Ly}\alpha} \exp[(i - i_0)\Delta \ln\nu]. \quad (16)$$

A. Transport in the Lyα line

Here we describe the computation of each term in Eq. (15).

1. Emission

We next consider the true emission of Lyα photons. In the case of emission, the photons arise via two-photon decays from the $n \geq 3$ states, Eq. (7). In the limit where we are close enough to Lyα line center to neglect the other resonances and the variation in photon phase space factors across the line, we may write this as

$$\dot{N}_i|_\mathrm{em}^\mathrm{R} = \sum_u x_u \Gamma_{u\rightarrow 2p} P_{2p\rightarrow 1s} \phi_\mathrm{V}(\nu_i) \Delta\nu_i. \quad (17)$$

This is a sum over all higher-energy states of hydrogen u, where $\Gamma_{u\rightarrow 2p}$ is the rate per second at which those states decay to the $2p$ state, $\phi_\mathrm{V}(\nu)$ is the Voigt distribution, $P_{2p\rightarrow 1s}$ is the branching fraction for $2p$ to decay to the ground level ($P_{2p\rightarrow 1s} = 1$ in vacuum), and $\Delta\nu_i$ is the bin width.

Rather than keep track of all the variables necessary to make that calculation, we retrieve the Lyα production rate

in photons per hydrogen atom per Hubble time from the interface (Sec. III B). Equation (17) simply reduces to

$$\dot{N}_i|^{\rm R}_{\rm em} = H\Pi\phi_{\rm V}(\nu_i)\Delta\nu_i, \tag{18}$$

where

$$\Pi = \frac{1}{H}\sum_u x_u\Gamma_{u\to 2p}P_{2p\to 1s} \tag{19}$$

denotes the Lyman-α production rate.

In reality the neglect of photon phase space factors and other resonances in Eq. (18) is not correct to the desired accuracy. We have thus implemented a ''corrected'' form of the equation,

$$\dot{N}_i|_{\rm em} = H\Pi\mathcal{E}(\nu_i)\phi_{\rm V}(\nu_i)\Delta\nu_i, \tag{20}$$

where $\mathcal{E}(\nu)$ is the correction function. It should be given by

$$\mathcal{E}(\nu) = \frac{\sum_{nl} x_{nl}(d\Lambda_{nl}/d\nu)(1+f_{\nu'})}{\sum_{nl} x_{nl}(d\Lambda^{\rm R}_{nl}/d\nu)(1+f_{nl,2p})}, \tag{21}$$

where $d\Lambda^{\rm R}_{nl}/d\nu$ is the resonance profile approximation to $d\Lambda_{nl}/d\nu$, i.e.

$$\frac{d\Lambda^{\rm R}_{nl}}{d\nu} = \frac{512\alpha_{\rm fs}^6\nu_{nl,2p}^3}{19\,683(2l+1)\mathcal{R}a_0^2}\frac{|\langle nl||r||2p\rangle|^2}{(\nu-\nu_{{\rm Ly}\alpha})^2}. \tag{22}$$

[This equation is derived from Eq. (B5) of Ref. [19], taking only the leading-order $(\nu-\nu_{{\rm Ly}\alpha})^{-2}$ term and recalling that $\langle 2p||r||1s\rangle = 2^{15/2}a_0/3^{9/2}$ and $\nu_{{\rm Ly}\alpha} = \frac{3}{4}\mathcal{R}$.] There should technically be stimulated emission factors of $1+f_\nu$ and $1+f_{{\rm Ly}\alpha}$ in Eq. (21), but in the vicinity of Lyα $f_\nu < 10^{-11}$ during our period of integration so we leave these out. Also $\mathcal{E}(\nu)$ should technically be computed in the rest frame of the hydrogen atom rather than in the comoving frame, but since $\mathcal{E}(\nu)$ varies extremely slowly with frequency (it does not possess a resonance at Lyα) this correction is unimportant.

Note that in Eq. (21), the $2s$ level should be included in the numerator since it is possible for a $2s\to 1s$ two-photon decay to produce emission within the frequency range of the Fokker-Planck code. In the blue wing of Lyα ($\nu > \nu_{{\rm Ly}\alpha}$), one should replace this with the $2s\to 1s$ Raman scattering rate,

$$\frac{d\Lambda_{2s}}{d\nu}(1+f_{\nu'}) \to \frac{dK_{2s}}{d\nu}f_{\nu'}. \tag{23}$$

[Note that there is no need to include $2s$ in the denominator, since the resonance approximation for its decay rate, Eq. (22), is zero.] Technically one should also include continuum states in the sum, but since the true two-photon emission is dominated by decays from $n\geq 3$ states rather than direct decays from the continuum we will not include the latter here.

Equation (21) is in general quite complicated. It can be evaluated under the approximation of Boltzmann equilibrium of the low-lying excited states. (The biggest exception to this rule is the $2s$:$2p$ ratio, which deviates from statistical equilibrium by 0.1% at $z=1190$, 1% at $z=950$, and 10% at $z=790$. The $3s$:$2p$, $3p$:$2s$, and $3d$:$2p$ ratios remain in Boltzmann equilibrium to $<1\%$ throughout at all $z>700$.) This allows us to construct a function $\mathcal{E}(\nu,T)$. This can be split into two contributions

$$\mathcal{E}(\nu,T) = \mathcal{E}_{2s}(\nu,T) + \mathcal{E}_{n\geq 3}(\nu,T) \tag{24}$$

coming from the $2s$ and $n\geq 3$ levels, respectively. Note that at $\nu=\nu_{{\rm Ly}\alpha}$ we must have $\mathcal{E}_{n\geq 3}\to 1$ and $\mathcal{E}_{2s}\to 0$. The function $\mathcal{E}(\nu,T)$ is fit to $<0.3\%$ accuracy over the range $|\vartheta|<0.01$ and $T<4700$ K, where $\vartheta = \nu/\nu_{{\rm Ly}\alpha}-1$, by

$$\mathcal{E}_{n\geq 3}(\nu,T) = e^{-5.4\vartheta} \tag{25}$$

and

$$\mathcal{E}_{2s}(\nu,T) = 92.5e^{6.0\vartheta}\frac{e^{h\nu_{{\rm H}\alpha}/T}|\vartheta|^3}{|e^{\vartheta h\nu_{{\rm Ly}\alpha}/T}-1|} \times \frac{1}{1+0.321e^{-h\nu_{{\rm Pa}\alpha}/T}}. \tag{26}$$

[The first fraction in this equation is physically motivated by the low-energy photon phase space factor $\propto|\vartheta|^3$, the thermal stimulated emission $(1+f)$ or absorption (f) phase space density $1/|e^{\vartheta h\nu_{{\rm Ly}\alpha}/T}-1|$, and the Boltzmann enhancement of $n=2$ relative to $n=3$ levels $e^{h\nu_{{\rm H}\alpha}/T}$. The second fraction takes into account the fact that some of the Lyα emission is preceded by Hβ emission from the $n=4$ levels, with $e^{-h\nu_{{\rm Pa}\alpha}/T}$ representing the Boltzmann suppression of $n=4$ relative to $n=3$ hydrogen atoms.]

The Voigt profile $\phi_{\rm V}(\nu)$ is computed using the integral formulation [38], except in the far damping wings where we switch to the asymptotic expansion for $|\nu-\nu_{{\rm Ly}\alpha}|\gg\sigma_\nu$.

2. Absorption

True absorption is the inverse process of true emission, so the same matrix element applies to both cases. In particular, the ratio of two-photon absorption from $1s$ to a given energy level u is related to the rate of emission via

$$\frac{\dot{N}|_{\rm em}}{\dot{N}|_{\rm ab}} = -\frac{g_{1s}x_u(1+f_\nu)(1+f_{\nu'})}{g_u x_{1s}f_\nu f_{\nu'}}, \tag{27}$$

where f_ν and $f_{\nu'}$ are the phase space densities associated with the two photons. We take ν to represent the frequency of the photon near Lyα and ν' to represent that of the low-frequency photon. Since the lower-frequency photon comes from a blackbody distribution, we have

$$\frac{1+f_{\nu'}}{f_{\nu'}} = e^{h\nu'/T_{\rm r}}. \tag{28}$$

Further assuming that the u level is in Boltzmann equilibrium with $2p$ (a good approximation for the $n \leq 4$ levels), we have

$$x_u = \frac{g_u}{g_{2p}} e^{-(E_u - E_{2p})/T_r}, \tag{29}$$

so

$$\frac{\dot{N}|_{em}}{\dot{N}|_{ab}} = -\frac{x_{2p}}{3x_{1s}f_\nu} e^{(-E_u + E_{2p} + h\nu')/T_r}. \tag{30}$$

Using conservation of energy to find that $h\nu' = E_u - E_{1s} - h\nu$, we can simplify this to

$$\frac{\dot{N}|_{em}}{\dot{N}|_{ab}} = -\frac{x_{2p}}{3x_{1s}f_\nu} e^{-h(\nu - \nu_{Ly\alpha})/T_r}. \tag{31}$$

This ratio applies for all of the excited states u, so it must apply to the total true emission and absorption rates as well. Thus we can solve for $\dot{N}_i|_{ab}$:

$$\dot{N}_i|_{ab} = -\frac{3x_{1s}f_\nu}{x_{2p}} e^{h(\nu_i - \nu_{Ly\alpha})/T_r} \dot{N}_i|_{em}. \tag{32}$$

We can simplify this further by defining the equilibrium number of photons per bin at line center,

$$N_{eq} \equiv \frac{8\pi\Delta \ln\nu}{n_H \lambda_{Ly\alpha}^3} \frac{x_{2p}}{3x_{1s}}, \tag{33}$$

from which we convert Eq. (32) into

$$\dot{N}_i|_{ab} = -\frac{N_i}{N_{eq}} \left(\frac{\nu_{Ly\alpha}}{\nu_i}\right)^3 e^{h(\nu_i - \nu_{Ly\alpha})/T_r} \dot{N}_i|_{em}. \tag{34}$$

Using Eq. (20), we arrive at

$$\dot{N}_i|_{ab} = -\frac{H\Pi\phi(\nu_i)\mathcal{E}(\nu_i)\Delta\nu_i}{N_{eq}} \left(\frac{\nu_{Ly\alpha}}{\nu_i}\right)^3 e^{h(\nu_i - \nu_{Ly\alpha})/T_r} N_i. \tag{35}$$

The value of N_{eq} is provided by the interface (Sec. III B).

3. Scattering

We now consider the change in frequency of photons due to resonant scattering off of hydrogen atoms, Eq. (9). The typical fractional change in frequency is roughly v_{th}/c where v_{th} is the rms thermal velocity of the hydrogen atoms. Nevertheless in a very optically thick line the net effect of many scatterings on the line profile may be important. We therefore write the Lyα transport in terms of a Fokker-Planck operator [33,34,39–41]. In formulating such an operator, it is essential to be sure that the scattering term exactly conserves photons and preserves the equilibrium distribution $f_\nu \propto e^{-h\nu/T_m}$ [40], even after discretization.

We define F_i to represent the net flux of photons from bin $i+1$ to bin i due to scattering. In this way we have

$$\dot{N}_i|_{sc} = F_i - F_{i-1}. \tag{36}$$

This formulation guarantees exact conservation of photons even in the discretized problem. In Fokker-Planck problems the fluxes are linear in the number of photons and its frequency derivative, i.e. in N_i and $N_{i+1} - N_i$, so we write

$$F_i = -\zeta_i N_i + \eta_i N_{i+1}, \tag{37}$$

where ζ_i and η_i are coefficients to be determined. In the equilibrium modified blackbody distribution, and for logarithmically spaced bins $\Delta\nu_i \propto \nu_i$, we have

$$N_i \propto \nu_i^3 e^{-h\nu_i/T_m}, \tag{38}$$

so in order for this to give zero net flux, we must have

$$\frac{\zeta_i}{\eta_i} = \frac{\nu_{i+1}^3}{\nu_i^3} e^{-h(\nu_{i+1} - \nu_i)/T_m}. \tag{39}$$

Equation (39) provides one constraint for two free parameters ζ_i and η_i. The other constraint must come from fixing the diffusion coefficient $\mathcal{D}(\nu)$ to the correct value. We see that

$$\dot{N}_i|_{sc} = \zeta_{i-1}N_{i-1} - (\zeta_i + \eta_{i-1})N_i + \eta_i N_{i+1}; \tag{40}$$

Taylor-expanding N_i allows us to write

$$\dot{N}_i|_{sc} = \frac{1}{2}(\eta_i + \zeta_{i-1}) \frac{\partial^2 N_i}{\partial i^2} + \text{0th, 1st derivatives}, \tag{41}$$

so the diffusion coefficient is $\frac{1}{2}(\eta_i + \zeta_{i-1})$ bin^2 s^{-1}. This can be written in the usual units of Hz^2 s^{-1} by multiplying by the square of the bin width,

$$\mathcal{D}(\nu) = \frac{1}{2}(\eta_i + \zeta_{i-1})\Delta\nu^2. \tag{42}$$

We then compare to the actual diffusion coefficient [41]

$$\mathcal{D}(\nu) = H\nu_{Ly\alpha}\sigma_\nu^2\tau_{Ly\alpha}f_S\phi_V(\nu), \tag{43}$$

where $\sigma_\nu^2 = \nu_{Ly\alpha}^2 T_m/(m_H c^2)$ is the variance of the Doppler shift distribution due to motion of H atoms. The fraction of Lyα absorptions that result simply in scattering (as opposed to true absorptions) is f_S; it is close to unity throughout the calculation, but a correct value is provided by the interface.

Since ζ_i and η_i are slowly varying functions, we may replace $\zeta_{i-1} \to \zeta_i$ in Eq. (42) and get

$$\frac{1}{2}(\eta_i + \zeta_i) = \frac{H\nu_{Ly\alpha}\sigma_\nu^2\tau_{Ly\alpha}\phi_V(\nu)}{\Delta\nu^2} \tag{44}$$

or

$$\eta_i + \zeta_i = \frac{H\nu_{Ly\alpha}\sigma_\nu^2\tau_{Ly\alpha}[\phi_V(\nu_i) + \phi_V(\nu_{i+1})]}{(\nu_{i+1} - \nu_i)^2}. \tag{45}$$

This and Eq. (39) are sufficient to determine ζ_i and η_i.

We handle the boundary conditions by disallowing any diffusion flux at either the red or blue boundary: $F_{-1} = F_{M-1} = 0$, where M is the number of bins.

The line profile for scattering, $\phi_V(\nu)$, is in principle modified by the existence of neighboring resonances such as Lyβ. However, comparison of the Voigt profile to the actual cross section for $1s \rightarrow 1s$ scattering shows errors of $<2\%$ in the frequency range of interest $|\vartheta| < 0.01$. Since the $1s \rightarrow 1s$ scattering makes only a $\leq 0.45\%$ correction to the recombination history, we ignore the ''correction to the correction.''

4. Hubble expansion and integration algorithm

For logarithmically spaced bins in frequency, it is easy to compute the effect of the Hubble expansion: when the Universe expands by an amount $\Delta \ln a = \Delta \ln \nu$, all photons simply shift into the next lowest frequency bin. Thus to account for the Hubble expansion, the contents of each bin are shifted down by one frequency bin at each time step:

$$N_i = N_{i+1} \qquad \text{(previous)}. \tag{46}$$

Since there are only a finite number of frequency bins, the values of the number density of photons that redshift into the highest-frequency bin must be determined by some other means. This value is denoted $N_{\rm in}$, and is provided by the interface (Sec. III B). This method of manually shifting photons to the left requires logarithmically spaced frequency bins and time steps. Moreover, the resolution $\Delta \ln \nu$ is tied to the time step. (Despite this restriction, this method has the advantage of avoiding spurious numerical diffusion, which would arise if the Hubble expansion term were simply written as a differential operator with a discretized derivative.)

Our method of solving Eq. (15) is thus to apply an implicit ODE solver (backward Euler) to the emission, absorption, and scattering terms in Eq. (15), evolve forward one time step, and shift the photons according to Eq. (46). We repeat this basic operation until we reach the desired final redshift $z_{\rm final}$.

The abundance of photons in the highest-frequency bin, N_{n-1}, is not specified by the above algorithm. Physically it is determined by the phase space density of photons redshifting into the line, in accordance with Eq. (14). This depends on the two-photon radiative transfer calculation and is provided by the interface code.

The emission, absorption, and scattering terms in the above equation can be written as a matrix equation,

$$\dot{N}_i|_{\rm em+ab+sc} = C_{ij} N_j, \tag{47}$$

where C_{ij} is a tridiagonal matrix. We step forward using a backward Euler method:

$$\frac{N_i(t+\Delta t) - N_i(t)}{\Delta t} = C_{ij}(t+\Delta t) N_j(t+\Delta t); \tag{48}$$

this is a first-order method but this is sufficient because of the extremely small time step. Inspection of the emission, absorption, and scattering terms shows that C_{ij} is tridiagonal and hence Eq. (48) is a tridiagonal linear system for $\{N_i(t+\Delta t)\}$. The $M \times M$ tridiagonal system can be solved by the usual $\mathcal{O}(M)$ complexity method of using the $i = 0$ equation to eliminate $N_0(t+\Delta t)$, then using the $i = 1$ equation to eliminate $N_1(t+\Delta t)$, and so on.

B. Interface

The evolution equation for the $\{N_i\}$ is only part of the recombination problem; it must interface to the multilevel atom code with the proper boundary conditions. This problem is considered here. The basic approach is iterative: the multilevel atom code is run first, to generate a table of input data for the Fokker-Planck code. Then the outputs of the Fokker-Planck code are used to apply corrections to the multilevel atom code, and so on until convergence is reached.

The data passed from the multilevel atom code to the Fokker-Planck code at each time step are:

(1) The matter and radiation temperatures.
(2) The $2p$ state width Γ_{2p} (inverse lifetime including all processes that depopulate the state, including Lyα decay, and bound-bound and bound-free absorptions);
(3) The true emission rate of Lyα photons $\Pi(a)$, computed using Eq. (19).
(4) The equilibrium abundance of Lyα photons $N_{\rm eq}/\Delta \ln \nu$, computed using Eq. (33).
(5) The abundance of photons redshifting into the Fokker-Planck grid region per H nucleus per Hubble time, i.e. $N_{M-1}/\Delta \ln \nu$ at ν_{M-1}.
(6) The fraction $f_{\rm inc}$ of Lyα absorptions that result in true absorption instead of scattering. This is determined by the branching ratios for transitions out of the $2p$ level of hydrogen. Note that $f_S = 1 - f_{\rm inc}$.
(7) The optical depth to scattering in Lyα photons, $\tau_{{\rm Ly}\alpha} f_S$.

In order to complete the iteration cycle, the Fokker-Planck code must return the corrections to Lyα transport to the MLA code. This is done in several steps. First, we turn off the two-photon transitions in the MLA code involving frequencies between ν_0 and ν_{M-1}. Then we correct the usual equations for the Lyα line with correction factors that cause it to produce the same outputs (net $2p \rightarrow 1s$ decay rate and photon phase space density at ν_0) as the Fokker-Planck code. Explicitly, the standard equation for the Lyα decay rate is

$$\dot{x}_{2p\rightarrow 1s,{\rm std}}(a) = \frac{8\pi H}{n_{\rm H} \lambda_{{\rm Ly}\alpha}^3} \frac{x_{2p}}{3 x_{1s}} - \frac{N_{\rm in}[(\nu_{{\rm Ly}\alpha}/\nu_{M-1})a]}{\Delta \ln \nu}, \tag{49}$$

where the rate of incoming photons is measured at the

frequency $\nu_{M-1} > \nu_{\mathrm{Ly}\alpha}$ at an earlier time since these are the photons that will reach Lyα line center at scale factor a. [Compare to Eq. (12).] The standard equation for the rate at which photons redshift out of Lyα is

$$f_{\mathrm{Ly}\alpha-,\mathrm{std}}(a) = \frac{x_{2p}}{3x_{1s}}. \tag{50}$$

We replace these with the equations

$$\dot{x}_{2p\to 1s}(a) = \xi_1(a)\dot{x}_{2p\to 1s,\mathrm{std}}(a) \tag{51}$$

and

$$f_{\mathrm{Ly}\alpha-}(a) = \xi_2(a) f_{\mathrm{Ly}\alpha-,\mathrm{std}}(a). \tag{52}$$

The correction factors $\xi_1(a)$ and $\xi_2(a)$ are determined by the Fokker-Planck code as follows. The net decay rate is $\dot{x}_{2p\to 1s}(a) = \sum_{i=0}^{M-1} \dot{N}_i|_{\mathrm{em+ab+sc}}$. This equation is unstable as written if $\dot{N}_i$ is determined by plugging N_i into the evolution equations. The stable method is to find the change ΔN in $\sum_{i=0}^{M-1} N_i$ before and after the em + ab + sc time step, and write

$$\dot{x}_{2p\to 1s}(a) = \frac{H\Delta N}{\Delta \ln \nu}. \tag{53}$$

We can then find $\xi_1(a) = \dot{x}_{2p\to 1s}(a)/\dot{x}_{2p\to 1s,\mathrm{std}}(a)$.

The red wing radiation correction factor $\xi_2(a)$ can be obtained by examining the phase space density of radiation emerging from the red wing of the line. In the MLA code with correction factor, this phase space density at ν_0 will be

$$f\left(\nu_0, \frac{\nu_{\mathrm{Ly}\alpha}}{\nu_0} a\right) = \xi_2(a) \frac{x_{2p}(a)}{3x_{1s}(a)}. \tag{54}$$

The true phase space density is however known from the Fokker-Planck code, so one can solve for $\xi_2(a)$.

Because $\xi_1(a)$ and $\xi_2(a)$ are correction factors and are generally close to unity, we expect faster convergence by having the Fokker-Planck code return $\xi_1(a)$ and $\xi_2(a)$ than absolute decay rates and phase space densities, so this is what we do.

The frequency spacing and time step in the Fokker-Planck code are $\Delta \ln \nu = \Delta \ln a = 8.5 \times 10^{-6}$, which is 5 times finer than the MLA code of Ref. [19] ($\Delta \ln a = 4.25 \times 10^{-5}$). Therefore the data provided by the MLA code are interpolated onto the finer grid required by the Fokker-Planck code.

We find that only two iterations of alternately running the Fokker-Planck and MLA codes are necessary. In our fiducial case, the first iteration leads to changes $|\Delta x_e|/x_e$ of at most 8.5×10^{-3}; the second iteration leads to a maximum change of 5.3×10^{-5}; and the third iteration 1.4×10^{-6}.

As a test, we have run the Fokker-Planck code with the scattering term $\dot{N}_i|_{\mathrm{sc}}$ turned off, and found agreement with the previous MLA code of Ref. [19], with a maximum error $|\Delta x_e/x_e|$ of 4×10^{-5} for $700 < z < 1600$.

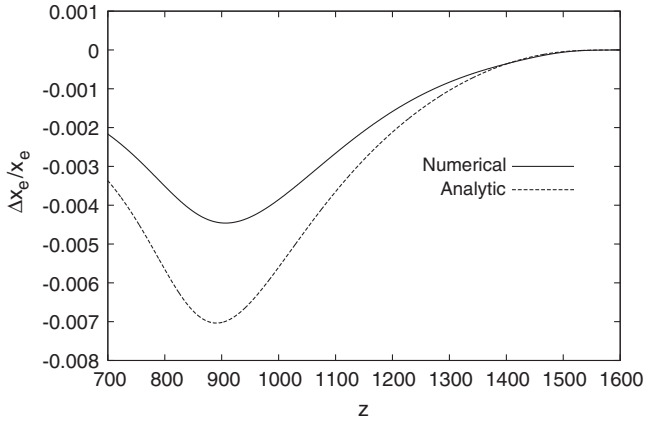

FIG. 2. The correction to the recombination history due to Lyα diffusion. The numerical computation of Sec. III is shown with a solid line, and Sec. IV with a dashed line. Recombination is accelerated due to the additional redshifting of photons via atomic recoil.

C. Results

The results from the Fokker-Planck code are shown in Fig. 2. This run began at $z_{\mathrm{init}} = 1605.5$. As expected from heuristic arguments (Sec. II C), the rate of recombination is accelerated by the inclusion of Lyα diffusion.

We have tested the convergence of our result with respect to the key numerical parameters. For example, if we only include scattering within ± 500 bins of the line center instead of the full ± 1000 bins, we find a maximum change in the ionization history $|\Delta x_e/x_e|$ of 10^{-5}. As an additional test, we tried using a $2.5\times$ coarser frequency binning for

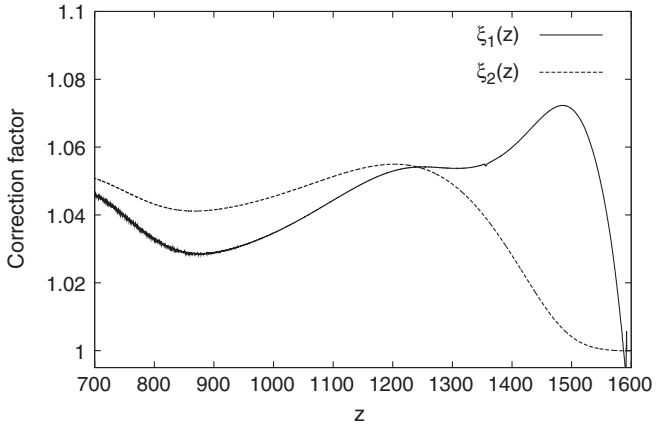

FIG. 3. The correction factors $\xi_1(z)$ and $\xi_2(z)$. The "standard" result for infinitesimally narrow Lyα line with no damping wing or diffusion effects is $\xi_1(z) = \xi_2(z) = 1$. Note that over most of the recombination history these are greater than 1, implying a faster $2p \to 1s$ decay rate but also more photons redshifting out of the Lyα line. The latter effect will lead to more two-photon absorption at low redshifts. [The glitch in $\xi_1(z)$ at $z \approx 1360$ is a startup transient from Lyβ at $z = z_{\mathrm{init}}$ redshifting into Lyα; given that the overall effect of the scattering correction is $<0.6\%$ in C_ℓ, this is far too small to affect CMB results.]

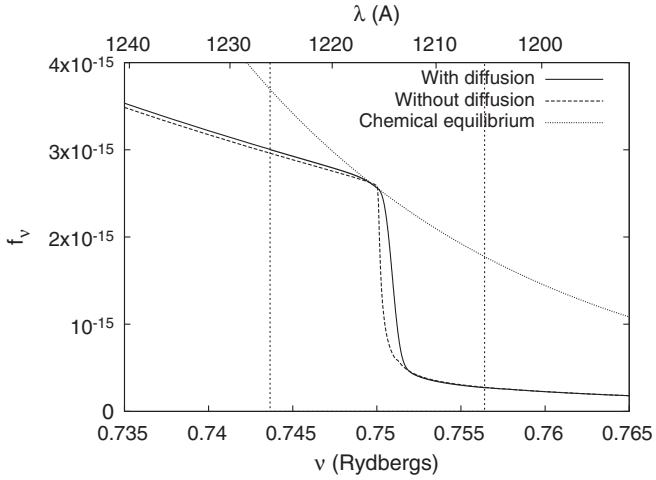

FIG. 4. The radiation spectrum in the vicinity of the Lyα line at $z = 1006$. The solid line shows the results of the diffusion code, and the dashed line shows the old code with no diffusion [19]. The vertical dotted lines show the boundaries of the Lyα diffusion region. The ''chemical equilibrium'' curve shows the approximation $f_\nu \approx (x_{2p}/3x_{1s})e^{-h(\nu-\nu_{\mathrm{Ly}\alpha})/T_\mathrm{r}}$ that should be valid in the immediate vicinity of line center. Note that $\nu_{\mathrm{Ly}\alpha} = 0.75$ Rydbergs.

the diffusion code (so that the diffusion code takes 2 instead of 5 time steps in each step of the MLA code). The frequency range remained the same, so this corresponds to parameters $\Delta \ln\nu = \Delta \ln a = 2.125 \times 10^{-5}$ and $M = 801$ bins. This modification leads to a maximum change in the ionization history $|\Delta x_e/x_e|$ of 5×10^{-5}.

The correction factors $\xi_1(z)$ and $\xi_2(z)$ are shown in Fig. 3.

We also show the radiation spectrum in Fig. 4. The radiation phase space density outside the diffusion code boundary (i.e. $\nu < \nu_0$ or $\nu > \nu_{M-1}$) is obtained from the MLA code with virtual levels as in Ref. [19], whereas for $\nu_0 \le \nu \le \nu_{M-1}$ we have used the phase space density from the diffusion code. We show the no-diffusion case (MLA + virtual levels only) with the dashed line. The most noticeable effect of the diffusion is the increased intensity at $\nu > \nu_{\mathrm{Ly}\alpha}$ due to Lyα photons diffusing to the blue side of the line. There is also an enhancement in the number of photons redshifting out of the line, which directly affects the recombination rate.

IV. ANALYTIC APPROXIMATION

We now consider a completely different approach to the Lyα diffusion problem, in which simple analytical calculations are used to estimate the correction to the Lyα escape rate. This approach is a valuable complement to the fully numerical method: it contains additional approximations, but it provides a better understanding of the physics and a check of the much more sophisticated Fokker-Planck code/interface. Analytic corrections (or more precisely, corrections based on reduction of the problem to a simple ODE) have been used by previous authors [34,35,42]. The specific implementation here is an extension of the two-photon analysis of Ref. [19] to include Lyα diffusion.

In Ref. [19] the problem of emission and absorption in the Lyα damping wings was considered with no diffusion (i.e. without considering the change in frequency during a $1s \to 1s$ scattering). The red and blue damping wings were handled separately since the radiative transfer phenomenology is different. In both cases, the equation for the radiation field is written down and is approximated by its time-steady form. Then:

(1) In the *red wing*, we find the correction to f_ν, and based on the concept of the flux of photons [Eq. (11)] we find a correction to the rate of Lyα escape. Since the correction is always positive [Eq. (12)] the red wing corrections always increase the recombination rate, leading to lower ionization fraction.

(2) In the *blue wing*, we find the number $x_+(t)$ of spectral distortion photons in the blue wing of Lyα per H nucleus according to the time-steady equation. This function starts at zero before recombination, reaches a positive maximum, and then declines to zero at late times as all photons redshift to lower frequencies. An additional downward decay rate $\dot{x}_{2p\to 1s} = \dot{x}_+(t)$ is grafted on to the MLA code to account for the $2p \to 1s$ decays that are required early during recombination to build the spectral distortion, and then the excitations that occur later during recombination as this distortion redshifts into Lyα. Note that this process accelerates recombination at early times ($\dot{x}_+ > 0$) but delays it later ($\dot{x}_+ < 0$).

We now extend the treatment of Ref. [19] in the red (Sec. IV A) and blue (Sec. IV B) wings. In all cases we neglect the variation in phase space density (i.e. factors of $\nu/\nu_{\mathrm{Ly}\alpha}$) across the Ly$\alpha$ line.

A. Red wing

Without frequency diffusion, the radiative transfer equation, Eqs. (82), (85), (87) of Ref. [19], is

$$\frac{\dot{f}_\nu}{H\nu} = \frac{\partial f_\nu}{\partial \nu} - \frac{\bar{W}}{(\nu - \nu_{\mathrm{Ly}\alpha})^2}\left[e^{h(\nu-\nu_{\mathrm{Ly}\alpha})/T_\mathrm{r}} f_\nu - \frac{x_{2p}}{3x_{1s}}\right], \tag{55}$$

where

$$\bar{W} = \frac{\tau_{\mathrm{Ly}\alpha}}{4\pi^2} \sum_{nl,n\ge 3} \frac{2l+1}{3} \frac{A_{nl,2p}}{e^{h\nu_{nl,2p}/T_\mathrm{r}} - 1} \tag{56}$$

is the width over which Lyα is optically thick to true absorption.

We can add the frequency diffusion to this equation by recalling the diffusion term [41],

$$\dot{f}_\nu|_{\rm sc} = \frac{\partial}{\partial\nu}\left[\mathcal{D}(\nu)\left(\frac{\partial f_\nu}{\partial\nu} + \frac{h}{T_{\rm m}} f_\nu\right)\right]. \quad (57)$$

[Note that the $(h/T_{\rm m})f_\nu$ term accounts for recoil.] In the far damping wings, we have

$$\mathcal{D}(\nu) \approx \frac{H\nu_{{\rm Ly}\alpha}\sigma_\nu^2\tau_{{\rm Ly}\alpha}f_{\rm S}A_{{\rm Ly}\alpha}}{4\pi^2(\nu-\nu_{{\rm Ly}\alpha})^2} \quad (58)$$

(see Ref. [41] and use the damping wing approximation to the Voigt profile for large $\nu - \nu_{{\rm Ly}\alpha}$). Adding this equation to Eq. (55) gives

$$\frac{\dot{f}_\nu}{H\nu} \approx \frac{\partial f_\nu}{\partial\nu} - \frac{\bar{W}}{(\nu-\nu_{{\rm Ly}\alpha})^2}\left[e^{h(\nu-\nu_{{\rm Ly}\alpha})/T_{\rm r}} f_\nu - \frac{x_{2p}}{3x_{1s}}\right] + \frac{\sigma_\nu^2\tau_{{\rm Ly}\alpha}f_{\rm S}A_{{\rm Ly}\alpha}}{4\pi^2}\frac{\partial}{\partial\nu}\left[\frac{1}{(\nu-\nu_{{\rm Ly}\alpha})^2}\left(\frac{\partial f_\nu}{\partial\nu} + \frac{h}{T_{\rm m}} f_\nu\right)\right]. \quad (59)$$

As in Ref. [19], we make the change of variables

$$\nu = \nu_{{\rm Ly}\alpha} + \frac{T_{\rm r}}{h} y \quad (60)$$

and

$$f_\nu = \frac{x_{2p}}{3x_{1s}}\Phi(y). \quad (61)$$

This, combined with dropping the $\dot{f}_\nu$ term (time-steady approximation) and taking $T_{\rm m} \approx T_{\rm r}$ (appropriate during the recombination era for the purposes of computing small corrections) simplifies Eq. (59) to

$$0 = \frac{d\Phi}{dy} - \frac{W}{y^2}(e^y\Phi - 1) + S\frac{d}{dy}\left[y^{-2}\left(\frac{d\Phi}{dy} + \Phi\right)\right], \quad (62)$$

where $W = h\bar{W}/T_{\rm r}$ and

$$S = \frac{\sigma_\nu^2\tau_{{\rm Ly}\alpha}f_{\rm S}A_{{\rm Ly}\alpha}h^3}{4\pi^2T_{\rm r}^3}. \quad (63)$$

This results in a dimensionless equation, Eq. (62), which depends on two constants W and S. The constant W determines the strength of the true absorption: the Lyα line is optically thick to true absorption out to frequencies $\nu_{{\rm Ly}\alpha} \pm WT_{\rm r}/h$. The constant S quantifies the importance of frequency diffusion relative to Hubble redshifting at frequencies $\nu_{{\rm Ly}\alpha} \pm T_{\rm r}/h$. In practice both are $\ll 1$.

Our time-steady equation, Eq. (62), is very similar to Eq. (93) of Ref. [19], and it satisfies the same boundary condition: $\Phi = 1$ at $y = 0$, since at line center we reach equilibrium and have $f_{\nu_{{\rm Ly}\alpha}} = x_{2p}/(3x_{1s})$. The second-order differential operator complicates the solution and necessitates an additional boundary condition that Φ not diverge as $y \to -\infty$. The numerical solution is presented in Appendix A. Just as in Ref. [19], the correction to the net $2p \to 1s$ decay rate is

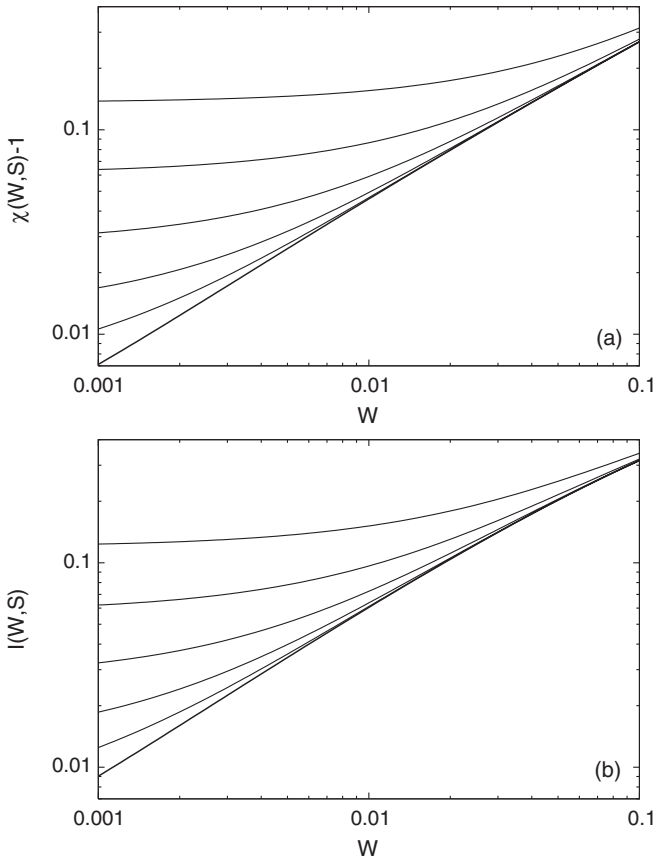

FIG. 5. (a) The analytic correction factors $\chi(W, S)$ and (b) $\mathcal{I}(W, S)$ associated with transport in the Lyα line. The thick bold line shows the factors without frequency diffusion, i.e. for $S = 0$. The thin lines show the factors for $S = 10^{-7}, 10^{-6}, 10^{-5}, 10^{-4}$, and 10^{-3} from bottom to top. Note that both emission/absorption in the far damping wings (parametrized by W) and frequency diffusion (parametrized by S) tend to increase the escape rate and the number of distortion photons in the Lyα blue wing, as expected.

$$\Delta\dot{x}_\downarrow = \frac{A_{{\rm Ly}\alpha}}{\tau_{{\rm Ly}\alpha}} x_{2p}(\chi - 1), \quad (64)$$

where $\chi \equiv \Phi(y = -\infty)$. The correction $\chi - 1$ is now a function of the two dimensionless constants, W and S. It is shown graphically in Fig. 5.

B. Blue wing

The frequency diffusion in the blue damping wing leads to a modification of the number of spectral distortion photons $x_+(t)$ per H atom in the blue wing of Lyα. As in Ref. [19], this can be approximated as

$$x_+ \approx \frac{8\pi\nu_{{\rm Ly}\alpha}^2 T_{\rm r}}{c^3 n_{\rm H} h}\int_0^\infty \Delta f_\nu dy, \quad (65)$$

where y is dimensionless frequency and Δf_ν is the distortion contribution to the phase space density. Writing the spectral distortion as

$$\Delta f_\nu = \left(\frac{x_{2p}}{3x_{1s}} - e^{-h\nu_{\mathrm{Ly}\alpha}/T_\mathrm{r}}\right)\Psi(y), \tag{66}$$

Ref. [19] showed that in the absence of frequency diffusion the rescaled spectral distortion $\Psi(y)$ satisfied the equation

$$\frac{d\Psi}{dy} = \frac{W}{y^2}(e^y\Psi - 1) \tag{67}$$

in the time-steady approximation, i.e. the same equation as occurs in the red wing. [This is Eq. (109) in Ref. [19]; the missing y^2 in that paper is a typo.] The inclusion of frequency diffusion proceeds exactly analogously to Sec. IV A, yielding

$$0 = \frac{d\Psi}{dy} - \frac{W}{y^2}(e^y\Psi - 1) + S\frac{d}{dy}\left[y^{-2}\left(\frac{d\Psi}{dy} + \Psi\right)\right]. \tag{68}$$

The abundance of distortion photons in the blue wing is then

$$x_+ \approx \frac{8\pi\nu_{\mathrm{Ly}\alpha}^2 T_\mathrm{r}}{c^3 n_\mathrm{H} h}\left(\frac{x_{2p}}{3x_{1s}} - e^{-h\nu_{\mathrm{Ly}\alpha}/T_\mathrm{r}}\right)\mathcal{I}(W,S), \tag{69}$$

where

$$\mathcal{I}(W,S) = \int_0^\infty \Psi(y)dy \tag{70}$$

is a dimensionless integral. Values of $\mathcal{I}(W,S)$ are computed according to the method in Appendix A and plotted in Fig. 5.

C. Implementation and results

Following the approach of Ref. [19], we first compute the Lyα transport parameters $W(z)$ and $S(z)$ for the pure MLA code with all two-photon transitions and scattering effects turned off. We then turn on the analytic corrections in Ref. [19] associated with the stimulated $2s \rightarrow 1s$ decays and nonthermal absorption, two-photon decays from $n \geq 3$ levels, and Raman scattering. The two-photon decays from $n \geq 3$ levels depended on the function $\chi(W) \equiv \Phi(y = -\infty|W)$ for the sub-Lyα decays (i.e. those in which both of the emitted photons have $\nu < \nu_{\mathrm{Ly}\alpha}$, which usually means one photon emerges in the red damping wing of Lyα) and $\mathcal{I}(W)$ for the super-Lyα decays (where one photon has $\nu > \nu_{\mathrm{Ly}\alpha}$, usually in the blue damping wing of Lyα). We can account for scattering semianalytically by replacing $\chi(W)$ and $\mathcal{I}(W)$ with their generalized values $\chi(W,S)$ and $\mathcal{I}(W,S)$ derived here. We may then compare the resulting recombination histories with and without Lyα scattering.

The transport parameters $W(z)$ and $S(z)$ are shown in Fig. 6.

The correction to the recombination history can be obtained by comparing the "old" $x_e(z)$ using $\chi(W)$ and $\mathcal{I}(W)$ without scattering to the "new" $x_e(z)$ using $\chi(W,S)$ and $\mathcal{I}(W,S)$. The correction is shown by the dashed line in Fig. 2. Note the qualitative agreement with the fully numerical result, although at low redshifts our analytic approximation overestimates the correction.

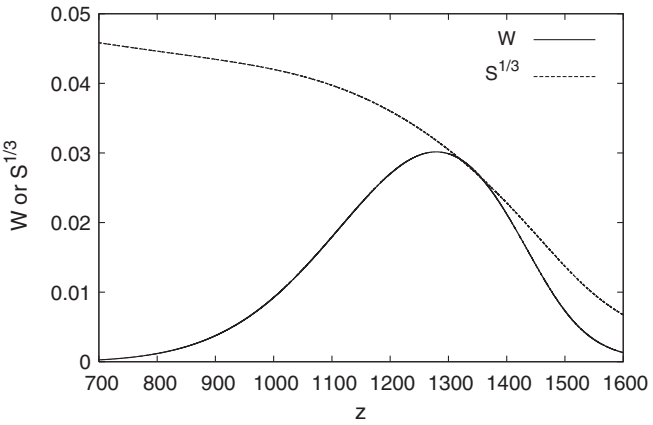

FIG. 6. The dimensionless Lyα transport parameters $W(z)$ and $S(z)$.

D. Comparison with other computations

The changes in the recombination history that we have found amount to corrections of at most 0.45%. This is less than the correction computed by several other authors. This section discusses some possible explanations for the apparent discrepancies. In some cases, the explanation lies with the fact that the corrections to the recombination history (or the effective escape probability) from emission/absorption in the damping wings are not additive with those from scattering—the net effect of including both is less than one would expect from adding the contributions to $\Delta x_e/x_e$. Also previous results on Lyα transfer did not include the deviation of emission versus absorption profiles, which can have a major impact on the results—e.g. without this we would have $\chi(W, S = 0) = 1$ for any W.

Chluba and Sunyaev [35] consider the time dependence of the radiation intensity in the Lyα line (i.e. nonquasistationarity) and the consequent effect on recombination. They include true emission and absorption in the damping wings but not scattering, and so in terms of the physics their result is most comparable to the treatment of two-photon decays by Hirata [19]. In particular, Hirata found that the dominant time-dependent correction was that associated with the blue damping wing of Lyα, i.e. with the time dependence of $\dot{x}_+$ (discussed here in Sec. IV B). Both Chluba and Sunyaev [35] (see their Fig. 12) and Hirata [19] (see his Fig. 8) find that the nonquasistationarity leads first to an accelerated recombination and then a delayed recombination as the spectral distortion redshifts through Lyα, but Chluba and Sunyaev find an effect up to a factor of $\sim$3 larger. We suspect this is due to their neglect of the deviation of emission versus absorption profiles, i.e. the e^y factor in Eq. (68). Without this factor (and with $S = 0$) we derive the solution $\Psi(y) = 1 - e^{-W/y}$ and hence the integral

$\mathcal{I}(W, S=0) = \int_0^\infty \Psi(y)dy = \infty$, and so the analytic approximation in Ref. [19] would yield an infinite correction in this approximation. Chluba and Sunyaev find a finite correction because of the finite duration of recombination (they use an exact treatment of nonquasistationarity rather than Hirata who treats the time dependence as a perturbation), but the effect is still large.

Grachev and Dubrovich [34] computed a correction to Lyα escape based on the modified escape probability of Grachev [42]. The latter did not include non-time-steady effects and was based on the rate of redshifting of Lyα photons out of the line, similar to our Sec. IV A. They also did not include the deviation of emission versus absorption profiles, which is equivalent to ignoring the e^y in our Eq. (62). This led them to the analytic approximation of Grachev [42], which is

$$\chi - 1 = \rho_{\rm G}\left[1 + \frac{\sigma_{\rm G}^2(4-\sigma_{\rm G}^2)}{3(2+\sigma_{\rm G}^2)} + \frac{\sigma_{\rm G}^4}{6}\right]^{-1}, \qquad (71)$$

where Grachev's dimensionless parameters are $\sigma_{\rm G}^2 \equiv 3^{2/3}W/\sqrt{[3]S}$ and $\rho_{\rm G} \equiv \sqrt{[3]3S}$. [Grachev [42] uses $i(-\infty)$ in place of our χ.] We have integrated our equation by the method of Appendix A without the e^y factor and find that this agrees with Eq. (71) to better than 10% in the range of interest. We note that our change in χ due to scattering, $\chi(W,S) - \chi(W,0)$, is increased if we turn off this term, in qualitative agreement with the fact that Grachev and Dubrovich [34] find a larger change in the recombination history due to Lyα scattering.

V. IMPLICATIONS FOR CMB ANISOTROPIES

In Fig. 7, we evaluate the effect of the Lyα diffusion correction on the CMB anisotropies, i.e.

$$\frac{\Delta C_\ell^{TT}}{C_\ell^{TT}} = \frac{C_\ell^{TT}(\text{with scattering})}{C_\ell^{TT}(\text{without scattering})} - 1. \qquad (72)$$

Note that the two-photon transitions are turned on in both the "with diffusion" and "no-diffusion" cases. The CMB power spectrum is computed using the Boltzmann code CMBFAST [8]. The most obvious effect is the oscillation in $\Delta C_\ell/C_\ell$: these are due to a slight shift in the acoustic scale to higher ℓ since the faster recombination results in a higher-redshift surface of last scattering. The overall tilt is partly a result of the reduced Silk damping: the faster recombination gives less time for the acoustic oscillations to be damped by photon diffusion, and hence the small-scale perturbations are not as suppressed as in the standard scenario. Also the reduced electron density at $z \sim 900$ implies a lower optical depth after the surface of last scattering and hence less washing out of the small-scale features in the CMB. This latter effect is slightly overestimated by the analytic computation, which is why the analytic result (dashed line in Fig. 7) has a slightly larger high-ℓ power spectrum.

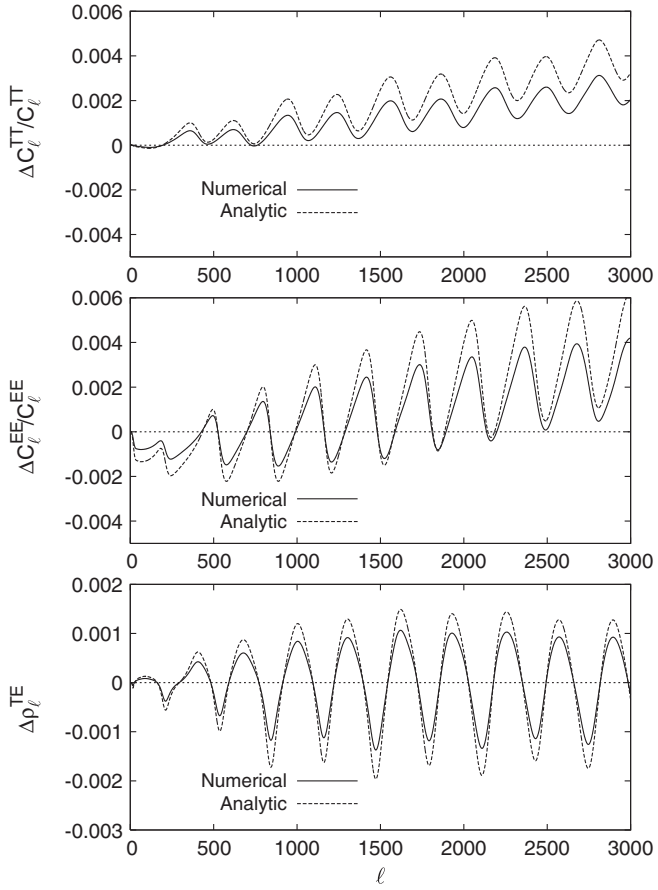

FIG. 7. The change in CMB power spectra for the temperature (top panel), polarization (middle panel), and the correlation coefficient (bottom panel) due to inclusion of Lyα scattering. The overall tilt and oscillating behavior are both the result of a faster recombination and hence higher redshift of the surface of last scattering: the tilt from the reduced Silk damping, and the oscillations due to the smaller acoustic horizon.

As in Ref. [19], we may evaluate the importance of the Lyα scattering correction for a given experiment by considering

$$Z^2 = \sum_{\ell\ell'} F_{\ell\ell'} \Delta C_\ell^{TT} \Delta C_{\ell'}^{TT}; \qquad (73)$$

here $F_{\ell\ell'}$ is the experiment's Fisher matrix and Z is the maximum number of sigmas by which any parameter fit could be affected. (An individual cosmological parameter may or may not be affected, depending on whether its effect on the CMB power spectrum is similar to that caused by the inclusion of scattering.) We consider the implications for the WMAP 2008 (5-year) data [3] (including beam and point source errors), the Arcminute Cosmology Bolometer Array Receiver (ACBAR) 2008 power spectrum [43] (including beam and calibration errors), and the upcoming *Planck* data as forecast using the noise curves for the 70 GHz (Low-Frequency Instrument) and 100 and 143 GHz (High-Frequency Instrument) channels

TABLE I. The magnitude of the correction Z (in number of sigmas) to the CMB power spectrum for several CMB experiments. This is shown both for the Lyα diffusion correction (center column) and for the combined two-photon decay corrections [19] and diffusion correction (right column).

Experiment	Z scattering	Z 2γ + scattering
WMAP 5 yr	0.07	0.23
ACBAR 2008	0.04	0.17
Planck	0.92	5.01

in the Blue Book [44] and assuming a usable sky coverage of $f_{\rm sky} = 0.7$.

Results of this analysis are displayed in Table I. It is seen that the correction due to Lyα scattering is small—it is only 0.9σ for *Planck*. Moreover, it goes in the opposite direction to the two-photon corrections found by Ref. [19] (the scattering raises the high-ℓ power spectrum whereas the two-photon corrections lower it).

VI. DISCUSSION

We have examined the effect of multiple scattering on the H I Lyα escape problem during the cosmological recombination epoch. Both numerical and analytic tools were developed to treat this problem simultaneously with emission and absorption in the damping wings. We find that scattering increases the escape probability and speeds up recombination because atomic recoil leads to a systematic shift of the photons to the red wing of the Lyα line. While this is in qualitative agreement with previous results [32,34], the magnitude of the scattering correction is less than previously suggested. We believe this is because the proper treatment of emission and absorption leads to a smaller effect from scattering. The modified treatment of the H I Lyα resonance results in a very small correction to the CMB power spectrum, ranging from zero to 0.4% at $\ell < 3000$, of the order of 0.9σ for *Planck*.

Our ultimate goal in hydrogen recombination is to develop a complete theory with an error budget as has been done for helium [28]. This will be based in part on the work presented in this paper, but will also require investigation of many minor radiative and collisional processes. Eventually the theory must be encapsulated in a code fast enough to use in Markov chain parameter estimation techniques, which could be the result of either analytic simplifications or interpolation codes [45].

ACKNOWLEDGMENTS

We thank Y. Ali-Haïmoud, D. Grin, and E. Switzer for useful discussions and comments. This project was supported by the U.S. Department of Energy (DE-FG03-92-ER40701) and the National Science Foundation (AST-0807337). C. H. is supported by the Alfred P. Sloan Foundation. J. F. received support from Caltech and the Flintridge Foundation.

APPENDIX A: SOLUTION TO TIME-STEADY DIFFUSION EQUATION

In this appendix, we consider the solution to the dimensionless time-steady radiative transfer equation, Eq. (62). In the red damping wing, $y < 0$, we desire the value of the solution at large negative values $\Phi(-\infty)$. In the blue wing, $y > 0$, we desire the integral $\int_0^\infty \Phi(y)dy$. Our ODE is different from the case of no frequency diffusion [19] because the diffusion operator renders it second-order. It can be solved by defining the variable

$$\Xi = Sy^{-2}\left(\frac{d\Phi}{dy} + \Phi\right). \tag{A1}$$

Here $\Xi(y)$ can be thought of as a dimensionless flux of photons passing through y due to frequency diffusion ($Sy^{-2}d\Phi/dy$) and recoil ($Sy^{-2}\Phi$). It is exactly zero without the diffusion/recoil terms. This leads to the linear system

$$\begin{aligned} \frac{d\Phi}{dy} &= \frac{y^2}{S}\Xi - \Phi, \\ \frac{d\Xi}{dy} &= Wy^{-2}(e^y\Phi - 1) - \frac{y^2}{S}\Xi + \Phi, \end{aligned} \tag{A2}$$

which is singular at $y = 0$.

We then implement a shooting method in the red damping wing, and a numerically stable modification of the shooting method in the blue wing.

1. Red wing

First consider the red wing, $y < 0$. The boundary conditions are that $\Phi(y = 0) = 1$ and $\Phi(y = -\infty)$ is finite. In order for $\Phi(y = -\infty)$ to be finite, inspection of the first equation in Eq. (A2) shows that we must have $\Xi(y = -\infty) = 0$. Therefore given any choice of $\chi = \Phi(y = -\infty)$, we may construct a solution $\Phi(y|\chi)$ to Eq. (A2) by taking $\Phi = \chi$ and $\Xi = 0$ at large negative y and integrating toward $y = 0$ using a second-order implicit ODE integrator.

The problem remains to choose the correct value of χ. In general for small negative y, the behavior of the solution is that $\Phi(y)$ remains finite because of the y^2 suppression in the first equation of Eq. (A2), while $\Xi(y)$ can have a $\sim y^{-1}$ divergence as one can see from the second equation:

$$\lim_{y\to 0^-}\Phi(y) = \alpha, \qquad \Xi(y) = \frac{W(1-\alpha)}{y} + \mathcal{O}(y^0). \tag{A3}$$

The desired solution is that corresponding to the boundary condition $\alpha = 1$. As we integrate the solution $\Phi(y|\chi)$ toward $y = 0$, we can determine the value α as a function of χ. Since the ODE is linear, $\alpha(\chi)$ is a linear function of

χ, and it suffices to obtain $\alpha(\chi = 0)$ and $\alpha(\chi = 1)$. Then the desired value of χ that satisfies the line center boundary condition can be obtained by linear extrapolation:

$$\chi(\alpha = 1) = \frac{1 - \alpha(0)}{\alpha(1) - \alpha(0)}. \tag{A4}$$

Since the fundamental problem is to find $\Phi(y = -\infty)$, we may simply report $\chi(\alpha = 1)$.

B. Blue wing

The solution in the blue wing, $y > 0$, must satisfy the boundary conditions $\Phi(y = 0) = 1$ and $\Phi(y = +\infty) = 0$. As before, we will implement a shooting method in the $+y$ direction, i.e. starting at small positive $y = \epsilon$ and integrating toward $+\infty$. But here the numerical calculation is much trickier: whereas in the red wing the growing mode of Eq. (A2) had only a power-law divergence ($\Xi \propto y^{-1}$) as one approached line center, here the growing mode grows faster than exponentially. Therefore if we push to large positive y an overflow error occurs. More seriously, this growing mode implies that the correct initial condition $\Xi(y = \epsilon)$ cannot be well represented even in double precision.

A slow but effective way to solve this problem is to write a function that takes in an initial value of y_i and a dimensionless photon density $\Phi(y_i)$ at that point, and find the critical value $\Xi_c[y_i, \Phi(y_i)]$ of Ξ that satisfies the boundary condition at $y = +\infty$ (i.e. is nondivergent). Here Ξ_c can be determined by a shooting method using a second-order implicit ODE integrator with two trials, taking advantage of linearity, just as we did for the red wing. We also determine how far one can integrate before the dangerous growing mode kicks in. This can be found from the function

$$F[y|y_i, \Phi(y_i)] = \frac{\partial \Phi[y|y_i, \Phi(y_i), \Xi(y_i)]}{\partial \Xi(y_i)} \Bigg|_{\Xi(y_i)=\Xi_c} e^{y-y_i}, \tag{A5}$$

which takes the initial value $F(y_i) = 0$ and rises toward ∞ as y increases. We solve for $y_{th}[y_i, \Phi(y_i)]$ at which $F = 10^4$, i.e. where the growing mode has increased by 4 orders of magnitude. The exponential e^{y-y_i} is included because the physical solution has $\sim e^{-y}$ dependence at large y.

We then begin our solution to Eq. (A2) by starting at $y = \epsilon$, $\Phi(y) = e^{-\epsilon}$, and $\Xi(y) = \Xi_c(\epsilon, e^{-\epsilon})$. The implicit ODE integrator is used to integrate to larger y, but only until we reach y_{th}. Beyond this point the growing mode is dangerous, so we recompute the critical Ξ_c at $[y, \Phi(y)]$, take this as a new initial condition, and keep integrating until the new y_{th}. This procedure "resets" the unstable mode each time a threshold value y_{th} is reached.

At very large values of y, where the growing mode grows very quickly, the above procedure becomes very slow. Fortunately, we find that at this point Φ is well represented by the large-y asymptotic result $\Phi(y) \to e^{-y}$. We may then extract the integral $\mathcal{I}(W, S) = \int_0^\infty \Phi(y|W, S)dy$.

In the real Universe, the solution at very large values of y is not accurate because of the presence of other resonances (e.g. Lyβ is at $y \sim 8$ at $z = 1000$). Fortunately, these large values of y do not contribute significantly to the integral $\mathcal{I}(W, S)$ because of the e^{-y} suppression of the integrand; it is for this reason that the analytic approximation based on $\mathcal{I}(W, S)$ works so well.

[1] D. N. Spergel, R. Bean, O. Doré, M. R. Nolta, C. L. Bennett, J. Dunkley, G. Hinshaw, N. Jarosik, E. Komatsu, L. Page *et al.*, Astrophys. J. Suppl. Ser. **170**, 377 (2007).

[2] J. Dunkley, E. Komatsu, M. R. Nolta, D. N. Spergel, D. Larson, G. Hinshaw, L. Page, C. L. Bennett, B. Gold, N. Jarosik *et al.*, Astrophys. J. Suppl. Ser. **180**, 306 (2009).

[3] E. Komatsu, J. Dunkley, M. R. Nolta, C. L. Bennett, B. Gold, G. Hinshaw, N. Jarosik, D. Larson, M. Limon, L. Page *et al.*, Astrophys. J. Suppl. Ser. **180**, 330 (2009).

[4] W. Hu, Phys. Rev. D **65**, 023003 (2001).

[5] A. Albrecht, G. Bernstein, R. Cahn, W. L. Freedman, J. Hewitt, W. Hu, J. Huth, M. Kamionkowski, E. W. Kolb, L. Knox *et al.*, arXiv:astro-ph/0609591.

[6] A. Albrecht, L. Amendola, G. Bernstein, D. Clowe, D. Eisenstein, L. Guzzo, C. Hirata, D. Huterer, R. Kirshner, E. Kolb *et al.*, arXiv:0901.0721.

[7] H. V. Peiris, E. Komatsu, L. Verde, D. N. Spergel, C. L. Bennett, M. Halpern, G. Hinshaw, N. Jarosik, A. Kogut, M. Limon *et al.*, Astrophys. J. Suppl. Ser. **148**, 213 (2003).

[8] U. Seljak and M. Zaldarriaga, Astrophys. J. **469**, 437 (1996).

[9] A. Lewis, A. Challinor, and A. Lasenby, Astrophys. J. **538**, 473 (2000).

[10] U. Seljak, N. Sugiyama, M. White, and M. Zaldarriaga, Phys. Rev. D **68**, 083507 (2003).

[11] P. J. E. Peebles, Astrophys. J. **153**, 1 (1968).

[12] Y. B. Zeldovich, V. G. Kurt, and R. A. Syunyaev, Zh. Eksp. Teor. Fiz. **55**, 278 (1968) [Sov. Phys. JETP **28**, 146 (1969)].

[13] S. Seager, D. D. Sasselov, and D. Scott, Astrophys. J. Lett. **523**, L1 (1999).

[14] S. Seager, D. D. Sasselov, and D. Scott, Astrophys. J. Suppl. Ser. **128**, 407 (2000).

[15] V. V. Sobolev, *Moving Envelopes of Stars* (Cambridge, MA: Harvard University, 1960).

[16] V. K. Dubrovich and S. I. Grachev, Astron. Lett. **31**, 359 (2005).

[17] W. Y. Wong and D. Scott, Mon. Not. R. Astron. Soc. **375**, 1441 (2007).
[18] J. Chluba and R. A. Sunyaev, Astron. Astrophys. **480**, 629 (2008).
[19] C. M. Hirata, Phys. Rev. D **78**, 023001 (2008).
[20] S. G. Karshenboim and V. G. Ivanov, Astron. Lett. **34**, 289 (2008).
[21] C. M. Hirata and E. R. Switzer, Phys. Rev. D **77**, 083007 (2008).
[22] E. R. Switzer and C. M. Hirata, Phys. Rev. D **77**, 083006 (2008).
[23] J. A. Rubiño-Martín, J. Chluba, and R. A. Sunyaev, Astron. Astrophys. **485**, 377 (2008).
[24] E. E. Kholupenko, A. V. Ivanchik, and D. A. Varshalovich, Mon. Not. R. Astron. Soc. **378**, L39 (2007).
[25] J. Chluba and R. A. Sunyaev, Astron. Astrophys. **446**, 39 (2006).
[26] E. E. Kholupenko and A. V. Ivanchik, Astron. Lett. **32**, 795 (2006).
[27] J. Chluba, J. A. Rubiño-Martín, and R. A. Sunyaev, Mon. Not. R. Astron. Soc. **374**, 1310 (2007).
[28] E. R. Switzer and C. M. Hirata, Phys. Rev. D **77**, 083008 (2008).
[29] A. Lewis, J. Weller, and R. Battye, Mon. Not. R. Astron. Soc. **373**, 561 (2006).
[30] W. Y. Wong, A. Moss, and D. Scott, Mon. Not. R. Astron. Soc. **386**, 1023 (2008).
[31] J. H. Krolik, Astrophys. J. **338**, 594 (1989).
[32] J. H. Krolik, Astrophys. J. **353**, 21 (1990).
[33] G. B. Rybicki and I. P. dell'Antonio, Astrophys. J. **427**, 603 (1994).
[34] S. I. Grachev and V. K. Dubrovich, Astron. Lett. **34**, 439 (2008).
[35] J. Chluba and R. A. Sunyaev, arXiv:0810.1045.
[36] J. Chluba and R. A. Sunyaev, Astron. Astrophys. **475**, 109 (2007).
[37] P. J. E. Peebles, *Principles of Physical Cosmology*, Princeton Series in Physics (Princeton University, Princeton, NJ, 1993).
[38] M. R. Zaghloul, Mon. Not. R. Astron. Soc. **375**, 1043 (2007).
[39] X. Chen and J. Miralda-Escudé, Astrophys. J. **602**, 1 (2004).
[40] G. B. Rybicki, Astrophys. J. **647**, 709 (2006).
[41] C. M. Hirata, Mon. Not. R. Astron. Soc. **367**, 259 (2006).
[42] S. I. Grachev, Astrophysics (English translation) **30**, 211 (1989).
[43] C. L. Reichardt, P. A. R. Ade, J. J. Bock, J. R. Bond, J. A. Brevik, C. R. Contaldi, M. D. Daub, J. T. Dempsey, J. H. Goldstein, W. L. Holzapfel *et al.*, arXiv:0801.1491.
[44] Planck Collaboration, The Scientific Programme of Planck, http://www.rssd.esa.int/Planck.
[45] W. A. Fendt, J. Chluba, J. A. Rubino-Martin, and B. D. Wandelt, Astrophys. J. Suppl. Ser. **181**, 627 (2009).